Journal of Structural Geology 32 (2010) 249–261

Contents lists available at ScienceDirect

Journal of Structural Geology

journal homepage: www.elsevier.com/locate/jsg

Superposed deformation fabrics in the Precambrian metabasic rocks of the Iron Ore Group, Singhbhum craton, Eastern India: Evidences from anisotropy of magnetic susceptibility studies

Gautam Ghosh [a,*], Snehalata Kumari [a], S.K. Patil [b], Joydip Mukhopadhyay [a], Arijit Ray [a]

[a] Department of Geology, Presidency College, Kolkata, India, 700073
[b] IIGM, Allahabad, UP, India

ARTICLE INFO

Article history:
Received 19 June 2009
Received in revised form
30 November 2009
Accepted 4 December 2009
Available online 11 December 2009

Keywords:
Archaean
Iron Ore Group
AMS
Superposed deformation
Singhbhum craton

ABSTRACT

Anisotropy of magnetic susceptibility (AMS) data have been utilized to build up the multiple deformation sequences and strain variation from an apparently undeformed metabasic lava sequence of the basal part of the Paleo-Mesoarchean greenstone succession of the Iron Ore Group rocks in the western Iron Ore basin, Singhbhum craton, eastern India. The basal lava crops out bordering the regional horseshoe shaped outcrop (the horseshoe synclinorium structure) of the overlying BIF rocks. AMS data of 892 cylindrical specimens drilled from 83 samples collected from different structural domains within the synclinorium structure are presented in the analysis. AMS orientation data have been analyzed in the light of superposed fold (Type-1 interference) fabrics developed within BIF as a result of successive deformation episodes (D_1 and D_2). It is found that the lava samples ubiquitously present two consistent magnetic fabrics homogeneous over smaller sub-areas, which have been successfully correlated with the D_1 and D_2 deformation fabrics from the BIF rocks. Moreover, a regional scale variation in intensity and nature of strain is noticed from the AMS data, which have been utilized to decipher folding mechanism as well as the changing deformation pattern during successive folding events.

1. Introduction

Identification and analysis of separate deformation episodes from a multiply deformed terrane is an important aspect of structural geology. It involves recognizing planar and linear fabrics of each deformation episode and studying their mutual relationships to ascertain the exact chronology and kinematics of deformation phases (Ramsay, 1967; Turner and Weiss, 1963; Ramsay and Huber, 1987; Thiessen and Means, 1980; Ghosh, 1966; Ghosh et al., 1992, 1993; Simon, 2004). However, usually practiced methods of geometrical analysis in a superposed terrane require presence of multiple sets of mesoscopic structures commonly manifested by folds, faults, foliations and lineations. In the absence of such planar and linear structures, identifying the separate deformation episodes and establishing the sequence and kinematics of deformations is a challenging task. The anisotropy of magnetic susceptibility studies (AMS) have been utilized in recent times in such cases to infer the deformation kinematics from terranes lacking any obvious deformation imprints (Hrouda, 1993; Tarling and Hrouda, 1993; Borradaile and Henry, 1997; Borradaile and Jackson, 2004). Deformation studies using AMS data in rocks like granites that do not contain well developed mesoscopic lineations and foliations have been extensively carried out (Bouchez et al., 1990; Archanjo et al., 1994; Leblanc et al., 1996; Bouchez, 1997; Djouadi et al., 1997; Borradaile et al., 1998; de Wall et al., 2001; Gleizes et al., 2001; Ferré et al., 2002; Neves et al., 2003; Sen et al., 2005; Parada et al., 2005; Sen and Mamtani, 2006). Besides, AMS studies have been successfully applied to analyse fold-thrust structures (Hrouda, 1978; Mamtani et al., 1999; Hrouda et al., 2000; Jayangondaperumal and Dubey, 2001; Mukherji et al., 2004) and record strain variations and strain gradients (Hrouda, 1993; Tarling and Hrouda, 1993; Borradaile and Henry, 1997; Mukherji et al., 2004) in deformed terranes.

However, AMS studies have not yet been used for establishing superposed deformation from strata that do not apparently exhibit megascopic evidences for multiple deformations though being a part of multiply deformed terrane. We document here, for the

* Corresponding author.
E-mail address: gautam0262@gmail.com (G. Ghosh).

0191-8141/$ – see front matter © 2009 Elsevier Ltd. All rights reserved.
doi:10.1016/j.jsg.2009.12.002

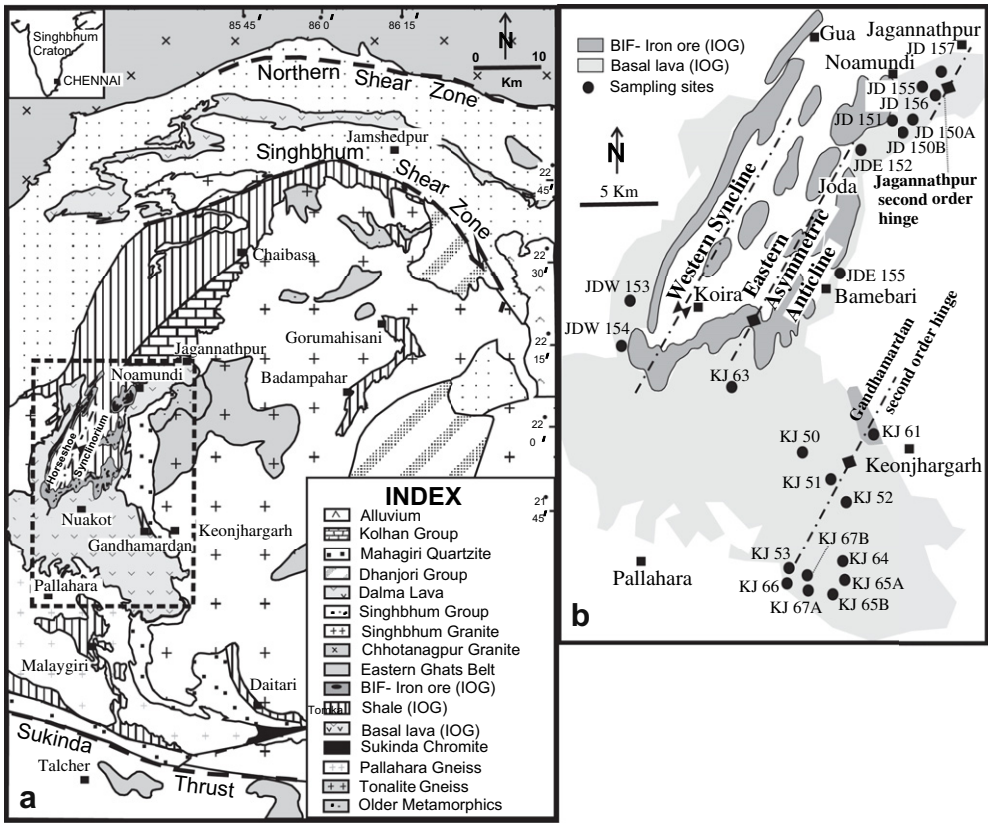

Fig. 1. (a) Geological map of the Singhbhum Craton (compiled from Saha, 1994; Sengupta et al., 1997). Present study area is marked by the dashed rectangle in the figure. (b) The simplified map of the horseshoe synclinorium showing the large scale and second-order folds. Locations of the 22 sites are also shown in the map (filled circles) from where all total 83 samples were collected for AMS analysis.

first time, evidences of superposed deformation from AMS studies of the metabasic lavas that are devoid of any mesoscopic deformational features from the Archaean greenstone belt succession of the Iron Ore Group, Singhbhum Craton, eastern India (Fig. 1a). The metabasic rocks form the basal unit of the Iron Ore Group (IOG) of rocks in the western Iron Ore basin (Jones, 1934; Saha, 1994; Ghosh and Mukhopadhyay, 2007; Beukes et al., 2008) around Noamundi–Koira Valley of the eastern Indian states of Jharkhand and Orissa. These are overlain by manganiferous shale, BIF-iron ore and an upper shale unit (Jones, 1934; Saha, 1994; Beukes et al., 2008). The western IOG rocks are disposed in a *horseshoe* shaped synclinorium structure (Jones, 1934; Dunn, 1929; Saha, 1994; Ghosh and Mukhopadhyay, 2007). Two episodes of deformation have been established from the BIF and host shale units of the IOG synclinorium (Jones, 1934; Dunn, 1940; Sarkar and Saha, 1962; Ghosh and Mukhopadhyay, 2007). However, the basal metabasic lava in most of the outcrop belts lack any mesoscopic deformation fabrics that prompted some workers to assign a younger Proterozoic age to these rocks (Sarkar and Saha, 1962; Saha, 1994). The primary objective of this contribution is to assess the extent of deformation in these apparently undeformed metabasic lavas through AMS studies and correlate the deformation history with that established from the marker BIF-unit of the synclinorium.

2. Geological background

The Singhbhum craton is one of the oldest Palaeo-Mesoarchean cratonic nuclei of the peninsular India (Saha, 1994). The craton is a composite mosaic of Archean greenstone-granitoids and Proterozoic supracrustal successions (Fig. 1a) (Acharyya, 1993; Saha, 1994; Sarkar, 2000; Mukhopadhyay, 2001; Naqvi, 2005; Misra, 2006). The Singhbhum Granite is the aerially most extensive unit, with three phases of emplacement between 3.3 Ga and 3.1 Ga (Saha, 1994; Misra, 2006), and encloses synformal keels of BIF-bearing greenstone belts, the Iron Ore Group (IOG) (Jones, 1934; Acharyya, 1993; Saha, 1994; Mukhopadhyay, 2001; Beukes et al., 2008), along its western (Noamundi–Koira), eastern (Gorumahisani–Badampahar) and southern (Malaygiri–Tamka–Daitari) peripheries (Fig. 1a), informally known as the western, eastern and southern IOGs, respectively. A minimum ~3.2 Ga age was provided for the Iron Ore Group by granitoids intrusive into the three outcrop belts (cf. Paul et al., 1991; Misra, 2006). Recently, Mukhopadhyay et al. (2008) obtained 3506 ± 2 Ma U-Pb SHRIMP zircon age from the dacitic lava of the southern IOG around Daitari and Basu et al. (2008) reported ~3.4 Ga age from the volcanics of the western IOG in the Noamundi–Koira Valley.

2.1. Western Iron Ore basin

The western IOG (Jones, 1934; Dunn, 1940; Sarkar and Saha, 1962; Saha, 1994) includes from base to the top, thick, massive, or pillowed metabasalt, lower phyllitic shale–tuff (locally with thin carbonates and manganiferous units), BIF-iron ore, and upper phyllitic shale (Ghosh and Mukhopadhyay, 2007; Beukes et al., 2008). Two phases of deformation structures have been described by most of the workers from this belt (Jones, 1934; Dunn, 1940; Sarkar and Saha, 1962; Saha, 1994; Ghosh and Mukhopadhyay, 2007). The main regional (D_1) structure comprises a low north-northeasterly plunging synclinorium, the '*horseshoe synclinorium*' (Fig. 1a), overturned towards east (Jones, 1934; Dunn, 1940; Sarkar

and Saha, 1962), which has been cross-folded (D_2) along an east-west axis (Jones, 1934; Sarkar and Saha, 1962; Ghosh and Mukhopadhyay, 2007). Chatterjee and Mukherjee (1981) and Mukherji et al. (2004), however, recognized a three phase deformation history with the earliest phase (D_1) represented by NW-SE to N-S trending very tight reclined to inclined folds that have been coaxially refolded by the regionally persistent N-S to NNE-SSW trending D_2 folds and a third generation of E-W trending cross folds (D_3 structures).

Saha (1994) suggested that the lava exposures in the western belt, particularly around Keonjhargarh and Jagannathpur where the outcrop of the lava body is much wide (Fig. 1a), comprises of an older deformed lava sequence belonging to the Archaean IOG rocks and a younger, undeformed lava sequence of probable Proterozoic age. However, as suggested previously by Jones (1934), Dunn (1940) and Sengupta et al. (1997), we too have failed to observe any notable difference among the lavas of the western belt both from field, petrographic and AMS studies. It appears that the lava unit can be mapped continuously around the horseshoe shaped BIF range to Keonjhar–Jagannathpur (Fig. 1a) and the contact between the supposedly older and younger lavas could nowhere be deciphered.

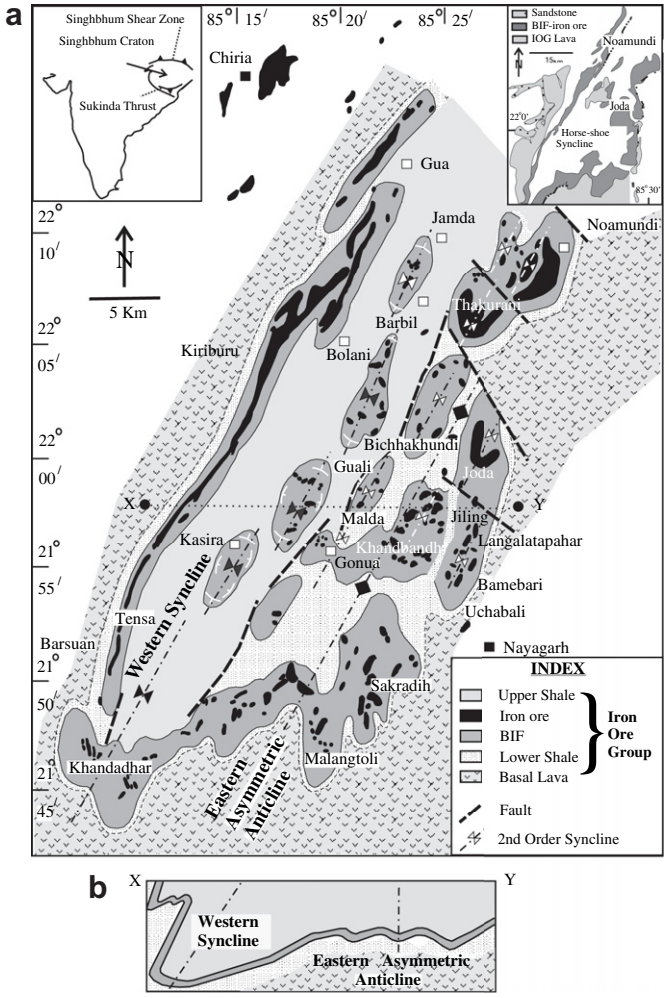

Fig. 2. (a) Map of the western Iron ore basin showing the distribution of different lithounits of the IOG sequence (modified after Ghosh and Mukhopadhyay, 2007). (b) Structural section, drawn along the line X–Y in Fig. 2a, depicts the western syncline- eastern asymmetric anticline fold pair developed within the IOG rocks.

3. Structural domains and deformation sequence in the western IOG

The geological map of the western IOG (Fig. 2a) modified by us (Ghosh and Mukhopadhyay, 2007) in the Noamundi–Koira valley reveals that the regional *horseshoe synclinorium* structure consists of a narrow *syncline* in the *west* and a broad *asymmetric anticline* in the *east* (Fig. 2a and b). A large database has been generated in course of the present study through structural analysis in several mines covering the entire outcrop belt of the horseshoe synclinorium structure. The details are beyond the scope of the present paper. However, a synoptic view of this analysis suggests two phases of fold and cleavage development from BIF-shale units (Ghosh and Mukhopadhyay, 2007). Superimposition of these two sets at high angles resulted in the development of dome-and-basin (*Type 1* superposed structures of Ramsay, 1967; Thiessen and Means, 1980; Ghosh et al., 1992; Ghosh et al., 1993) patterns in different scales (Ghosh and Mukhopadhyay, 2007). The detached elliptical BIF-iron ore outcrops in the wide subhorizontal *hinge zone* of the '*eastern anticline*' (Figs. 2a and 3), are typical examples of such macroscopic Type-1 interference patterns resulting from superimposition of the E-W folds on the regionally persistent N-NNE fold set (Ghosh and Mukhopadhyay, 2007).

However, the geometry (open-to-tight, isoclinal; upright-to-inclined, overturned) and orientation (axial traces vary from NNW-SSE to NE-SW) of early folds vary widely in comparison to the E-W trending open later folds. The variation in nature of the early folds from the area can be better explained by considering that the two interfering fold sets are not exactly at right angles to one another. In such cases of oblique superposition, an early fold (F_1) may either get tightened or open out depending upon the local orientation of the F_1 hinge line and axial surfaces with respect to the later shortening direction. Further it would also likely to develop a significant amount of rotation of F_1 fold axes

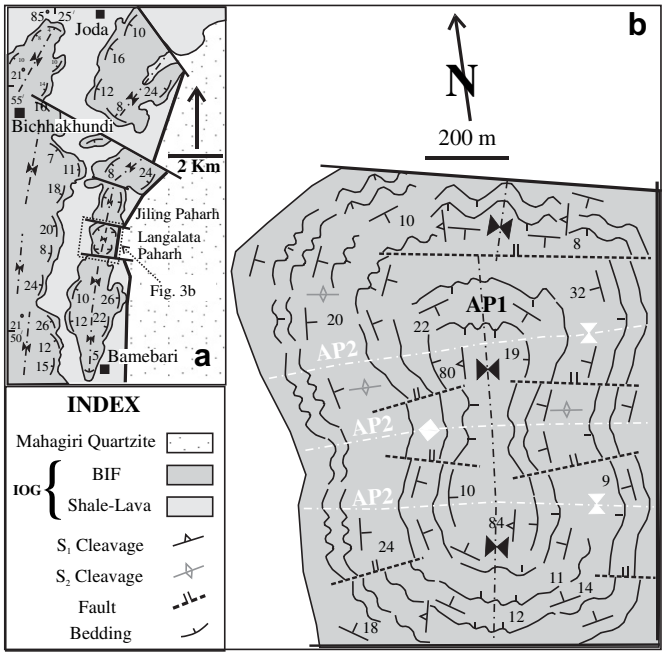

Fig. 3. (a) Geological map showing distribution of structural elements and lithounits in between Joda and Bamebari. The dotted rectangle represents the area where a large scale structural map (Fig. 3b) has been prepared. (b) Large scale structural map of the Langalatapahar iron mine exemplifying the elongated domal outcrop of the BIF-iron ore body.

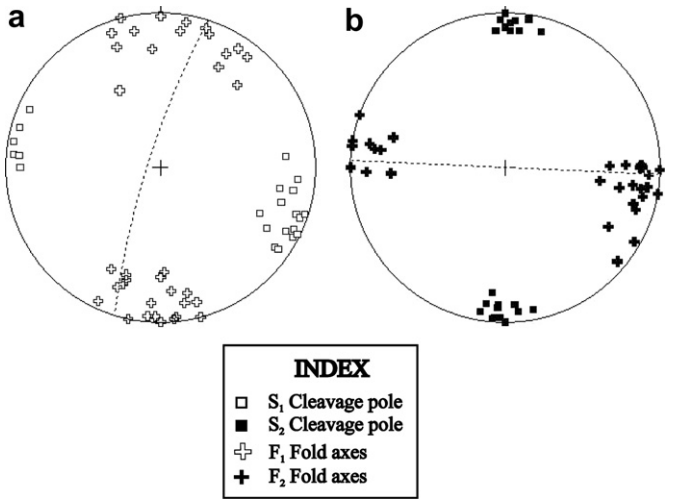

Fig. 4. Stereographic projections showing (a) distribution of N-S to NNE-SSW planar and linear structural elements within BIF at Gandhamardan iron mine. The girdle represents the average orientation of the S_1 cleavage as 018/83 W. (b) distribution of E-W planar and linear structural elements within BIF at Gandhamardan iron mine. The girdle represents the average orientation of the S_2 cleavage as 092/89 N.

and axial surfaces away from the direction of shortening (Sengupta et al., 2005). The wide variation in geometry and orientation of the early northerly trending fold set in the area led us to infer the variation in terms of an oblique superposition of the late E-W folds on the early NNE-SSW trending fold set. The dominance of Type 1 interference patterns in different scales and absence of any evidence for repetition of stratigraphy also support the above inference in contrast to the idea of an early coaxial deformation history as proposed earlier (e.g., Chatterjee and Mukherjee, 1981; Mukherji et al., 2004). The interpretation thus essentially leads to a two-phase deformational sequence, as suggested by some earlier workers (Jones, 1934; Dunn, 1940; Sarkar and Saha, 1962; Ghosh and Mukhopadhyay, 2007) in contrast to the idea of a three-phase deformation (Chatterjee and Mukherjee, 1981; Mukherji et al., 2004).

Large expanses of the basal lava body are exposed south and east of the regional horseshoe structure, around Keonjhargarh and Jagannathpur, respectively (Fig. 1b). The fault bounded isolated outcrop of BIF-iron ore at Gandhamardan mine near Keonjhargarh (Fig. 1b) depicts two interfering fold and cleavage sets (a NNE early fold set and a later E-W set; Figs. 4a and b and 5a) giving rise to the Type-1 interference pattern in mesoscopic scale (Fig. 5b). The gross sub-horizontal attitude of the enveloping surfaces of folds, high bedding-cleavage angle and nature of superposition in this isolated fault-bound outcrop clearly corresponds to the *hinge zone* of the northerly placed main outcrop belt of the '*eastern anticline*' (Fig. 1b). The lavas with subhorizontal flow layers (Fig. 6a) crop out below the folded BIF rocks in mine sections. Thus the overall structure around the Gandhamardan Mine has been interpreted as a sub-horizontal *second order hinge* (the *Gandhamardan second-order fold hinge*; Fig. 1b) developed on the eastern limb of the '*eastern anticline*'. Similarly, the lava outcrop in between Noamundi–Jagannathpur (Fig. 1b) with sub-horizontal attitude and both N-S and E-W warps (Fig. 6b) is interpreted as a *second order fold hinge* (named as the *Jagannathpur second-order fold hinge*; Fig. 1b) occurring due east of the main hinge zone of the '*eastern anticline*'. In contrast, narrow bands of the basal lava body along the western limb of the '*western syncline*' and eastern limb of the '*eastern anticline*', in spite of minor variations, show an overall westerly dip at moderate to low angles (Fig. 6c and d).

4. AMS studies

The main objective of the study was to analyze magnetic fabrics from the basal metabasic lava of the IOG rocks outcropping in and around the *regional horseshoe structure*. The basic lava is very fine grained, greenish in colour and mostly massive which locally grades to vesiculated, amygdular lava showing flow layering or pillow structures. It shows secondary foliation development locally at preferred structural sites such as the '*second order fold hinges*'. The lava throughout the outcrop belts of the western IOG essentially attains a low-greenschist facies metamorphic grade with mineral assemblages represented by actinolite, tremolite, clinopyroxene, albite, epidote, chlorite, sericite with accessories such as sphene, calcite and opaques. The massive lava in general is characterized by radially oriented actinolite–tremolite blades with relicts of variably altered pyroxene and albite phenocrysts (Fig. 7a). Schistosity where developed is defined either by preferred orientation of recrystalized chlorite–sericite flakes (Fig. 7b) or by a domain-microlithon fabric of actinolite–tremolite blades (Fig. 7c). The para- and diamagnetic minerals dominate over opaques (ferromagnetic component; $<$0.5 wt %) in these metalavas.

4.1. Sampling and measurement

A total of 83 oriented rock samples of the basal lava of the IOG sequence were collected from the study area from 22 sites across the *regional horseshoe fold structure* (Fig. 1b). The sites were precisely positioned with a GPS and care was taken to collect samples from different structural domains (Table 1). It shows that while several of the samples belong to the *hinge zone* of the regional folds, others belong to the *limbs* and *second-order hinges* of the

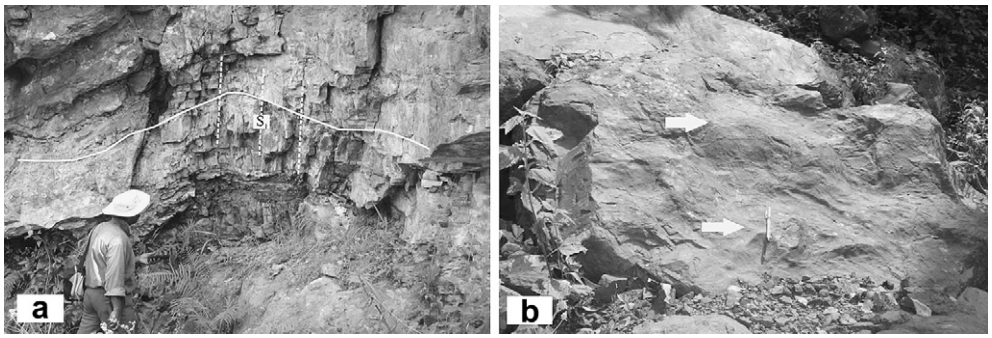

Fig. 5. Field photographs showing (a) folded outcrop of BIF with axial planar cleavage development near the hinge at Gandhamardan iron mine. (b) type 1 interference pattern within BIF outcrop at Gandhamardan iron mine. The arrows indicate position of minor domes.

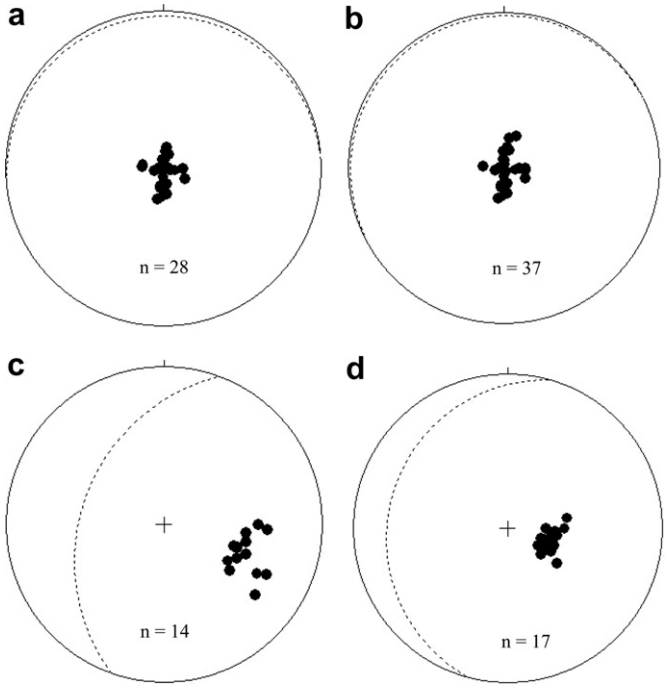

Fig. 6. Stereographic projections showing (a) poles to sub-horizontal flow layers within the basal lava exposed around Nuakot–Gandhamardan at the 'Gandhamardan second-order fold hinge'. The girdle represents the average orientation of the layering as 266/03 N. (b) poles to sub-horizontal flow layers within the basal lava exposed around Jagannathpur–Danguaposi at the 'Jagannathpur second-order fold hinge'. The girdle represents the average orientation of the layering as 243/02 NW. (c) poles to flow layers within the basal lava exposed around Barsuan at the western limb of the 'western syncline'. The girdle represents the average orientation of the layering as 020/46 W. (d) poles to flow layers within the basal lava exposed around Joda–Bamebari at the eastern limb of the 'eastern anticline'. The girdle represents the average orientation of the layering as 15/23 W. 'n' represents no. of flow layers measured in each 'structural setting'.

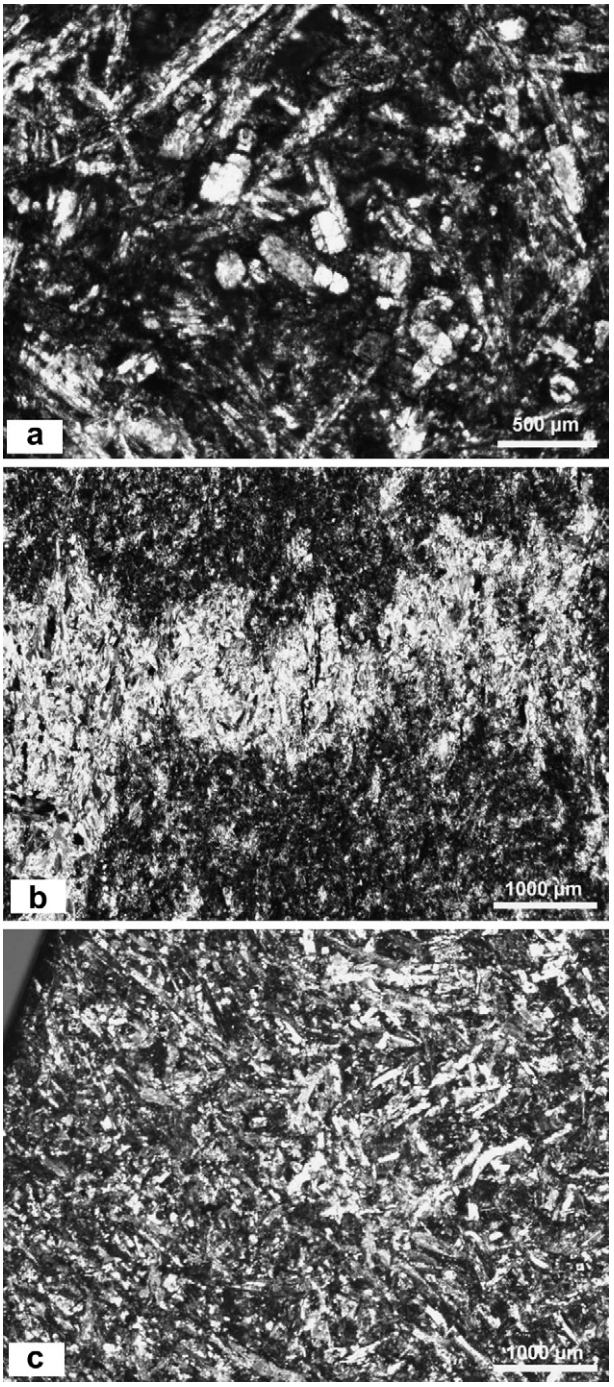

Fig. 7. Photomicrographs of lava samples showing the dominant texture in the massive variety as well as the schistose fabric developed during later deformation at preferred structural sites. (a) shows radially oriented actinolite–tremolite blades surrounding altered pyroxene and plagioclase phenocrysts in a massive metalava. (b) shows a folded layering within metalava and growth of chlorite–sericite flakes parallel to the axial planar direction defining a schistose fabric. (c) shows development of a domain-microlithon fabric within deformed metalava.

folds. For statistical treatment of AMS data multiple cores from each oriented sample were drilled and a total of 892 standard cylindrical specimens (22 mm long and 25 mm in diameter) were obtained by making 3–20 cores from each sample. The attitudes of layering in the field at these sites were also recorded.

Low field bulk susceptibility (K_m) and other AMS measurements (P_j, K_1, K_2 and K_3) were carried out using the KLY-2 and MFK-1 Kappabridge (Geofyzica Brno, Czech Republic) at the palaeomagnetic laboratory of Indian Institute of Geomagnetism (IIGM), Alibag and Allahabad, India. Each core was measured in 15 different directions to get the orientation and magnitudes of the principal axes K_1, K_2 and K_3 ($K_1 \geq K_2 \geq K_3$). From this basic data, the mean susceptibility (K_m), strength of magnetic lineation ($L = K_1/K_2$) and foliation ($F = K_2/K_3$), the corrected degree of anisotropy (P_j) and shape parameter (T_j) were determined (Jelinek, 1981; Tarling and Hrouda, 1993). The calculations of these parameters were carried out using Anisoft-3 software. P_j is a measure of the eccentricity of the magnetic susceptibility ellipsoid and T_j gives the shape of the susceptibility ellipsoid.

4.2. Magnetic mineralogy

Temperature dependent susceptibility studies were carried out on some representative samples (Fig. 8) to have an idea on the source of AMS in the rocks. Any appreciable change in magnetic susceptibility was absent during heating and cooling (Fig. 8a and b) of a few samples (JD 155 and KJ 63.1) indicating dominance of paramagnetic minerals. However, a very small component of magnetite could be expected in the other samples as the susceptibility drop was noticed at 580 °C (Fig. 8c–i). Most of these samples, belonging to sites KJ 50, KJ 67, JD 150, JDW 153 and JDW 154, showed increasing susceptibilities during the cooling, especially at 580 °C (Fig. 8). This behavior suggests the formation of new magnetite due to transformation of iron bearing paramagnetic minerals during the heating process of the experiment. Overall, it

Table 1
List of basal lava samples collected from 22 sites around the 'horseshoe synclinorium' structure in the western IOG basin. The position of each site with respect to the 'structural domains' in the western IOG basin and orientation of layering at each site are also specified in the table. Several samples were collected from each sampling site (represented by Sample no. in the third column from the left in the Table. Several core specimens were drilled out from each sample for palaeomagnetic measurements as shown in Table 2).

Locality	Site no.	Sample no.	Structural Domain
W-SW of Gandhamardan mine	KJ 50	KJ 50.1, KJ 50.2, KJ 50.3, KJ 50.4 KJ 50.5	Gandhamardan Second-order Fold Hinge
	KJ 51	KJ 51.1, KJ 51.2, KJ 51.3a, KJ 51.3b	
	KJ 52	KJ 52.1, KJ 52.2, KJ 52.3	
In between Keonjhargarh–Pallahara	KJ 53	KJ 53.1, KJ 53.2, KJ 53.3	
Gandhamardan iron mine	KJ 61	KJ 61.1, KJ 61.2	
Nuakot	KJ 63	KJ 63.1, KJ 63.2, KJ 63.3	Hinge- *Eastern Anticline*
In between Keonjhargarh–Pallahara	KJ 64	KJ 64.1, KJ 64.2, KJ 64.3, KJ 64.4a KJ 64.4b	Gandhamardan Second-order Fold Hinge
	KJ 65A	KJ 65A.1, KJ 65A.3, KJ 65A.4a KJ 65A.4b	
	KJ 65B	KJ 65B.2	
	KJ 66	KJ 66.1	
	KJ 67A	KJ 67A.1	
	KJ 67B	KJ 67B.1	
In between Joda–Danguaposi	JD 150 A	JD 150 A.1, JD 150 A.5	Jagannathpur Second-order Fold Hinge
	JD 150B	JD 150B.2, JD 150B.3, JD 150B.4	
South-east of Noamundi	JD 151	JD 151.1, JD 151.2, JD 151.3 JD 151.4, JD 151.5	Eastern limb, *Eastern Anticline*
North of Joda	JDE 152	JDE 152.1, JDE 152.2, JDE 152.3 JDE 152.4, JDE 152.5	
Barsua	JDW 153	JDW 153.1a, JDW 153.1c, JDW 153.2 JDW 153.3, JDW 153.4, JDW 153.5 JDW 153.6	Western limb *Western Syncline*
	JDW 154	JDW 154.1, JDW 154.2, JDW 154.3 JDW 154.4, JDW 154.5	
Bamebari	JDE 155	JDE 155.1, JDE 155.2, JDE 155.3 JDE 155.4, JDE 155.5, JDE 155.6	Eastern limb *Eastern Anticline*
In between Danguaposi–Jagannathpur	JD 155	JD 155.1, JD 155.2, JD 155.3 JD 155.4, JD 155.5	Jagannathpur Second-order Fold Hinge
	JD 156	JD 156.1, JD 156.2, JD 156.3 JD 156.4, JD 156.5, JD 156.6	
	JD 157	JD 157.1, JD 157.2, JD 157.3 JD 157.4, JD 157.5, JD 157.6	

could be summarized from temperature susceptibility experiments that paramagnetic minerals are the major magnetic minerals in the studied samples.

4.3. AMS data

The mean bulk susceptibility (K_m) values in the samples are in general low and vary from 333×10^{-6} to 1094×10^{-6} SI units (Table 2). The AMS strength and shape have been derived using the P_j and T_j parameters (Jelinek, 1981). The processing of the magnetic data involved preparation of Jelinek plots (Fig. 9) to investigate the type of strain the rocks were subjected to. Separate Jelinek plots were prepared for samples from different sites (Fig. 9a–e). The plots showed that data from rocks of the study area ranges from prolate to oblate field indicating an oblate to prolate shape of the susceptibility ellipsoid. A separate plot of P_j vs. K_m (Fig. 10) for the samples has been prepared to assess the role of magnetic susceptibility (K_m) behind degree of anisotropy (P_j).

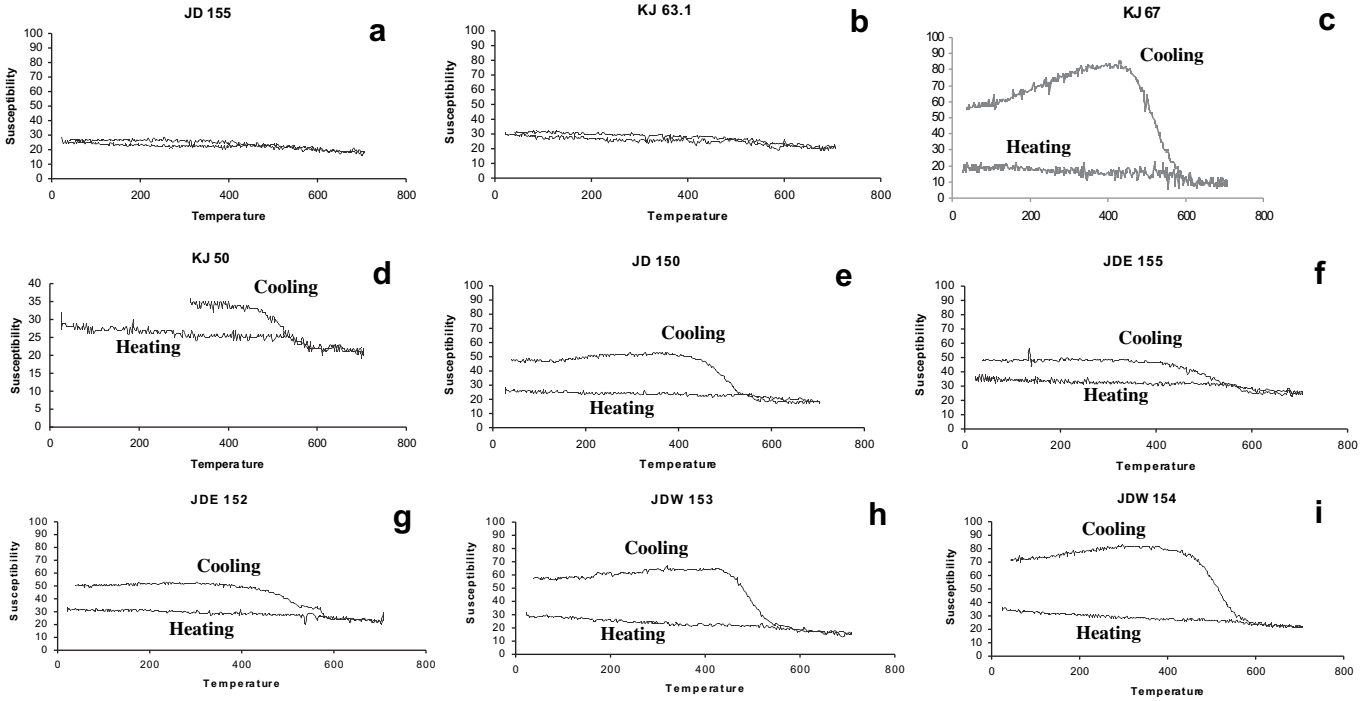

Fig. 8. Graphs showing variation of magnetic susceptibility with temperature during 'heating' and 'cooling' experiments performed on some representative samples (a–i) from the basal lava sequence of the IOG.

Table 2
AMS data of the 83 basal lava samples collected from 22 sites in the western IOG basin. (N- total no. of core specimens per sample; K_m- mean magnetic susceptibility in 10^{-6} SI units; F- magnetic foliation; L- magnetic lineation; Pj- corrected degree of anisotropy; Tj- shape parameter; D/I represents the direction and amount of dip of principal axes of magnetic ellipsoid). The parameters (K_m, F, L, P_j, T_j) represent the mean value of the core specimens measured for each sample.

Sample no.	Structural domain	N	Km ($\times 10^{-6}$ SI Unit)	L	F	P_j	T_j	K_1−D/I	K_3−D/I
KJ 50.1	**Gandhamardan**	12	333.53	1.004	1.005	1.009	0.14	175/15	276/36
KJ 50.2	**Second-order Fold Hinge**	6	346.35	1.002	1.012	1.016	0.672	194/1	284/2
KJ 50.3		8	483.96	1.003	1.01	1.013	0.57	181/14	289/50
KJ 50.4		11	503.8	1.012	1.005	1.017	−0.392	187/11	289/46
KJ 50.5		14	546.23	1.003	1.006	1.009	0.275	2/20	92/0
KJ 51.1		11	715.25	1.009	1.009	1.019	−0.03	344/61	137/26
KJ 51.2		10	734.84	1.01	1.012	1.023	0.08	234/34	114/38
KJ 51.3a		12	482.85	1.002	1.011	1.013	0.747	7/50	102/4
KJ 51.3b		9	427.63	1.005	1.01	1.015	0.341	15/74	272/4
KJ 52.1		12	575.18	1.02	1.011	1.032	−0.298	289/70	76/17
KJ 52.2		7	594.3	1.02	1.013	1.034	−0.199	288/71	66/14
KJ 52.3		12	584.7	1.017	1.011	1.028	−0.18	285/64	84/25
KJ 53.1		14	572.53	1.019	1.015	1.034	−0.108	346/63	252/2
KJ 53.2		14	553.13	1.022	1.019	1.042	−0.067	359/64	243/13
KJ 53.3		7	594.2	1.014	1.017	1.031	0.099	45/70	264/16
KJ 61.1		16	619.28	1.005	1.012	1.018	0.43	313/48	82/30
KJ 61.2		11	625.66	1.009	1.016	1.025	0.275	315/41	91/40
KJ 64.1		11	543.34	1.015	1.009	1.024	−0.264	226/4	327/72
KJ 64.2		15	596.55	1.012	1.011	1.023	−0.032	81/7	312/79
KJ 64.3		10	570.61	1.02	1.013	1.034	−0.222	60/13	263/76
KJ 64.4a		9	614.73	1.018	1.02	1.038	0.029	220/1	313/69
KJ 64..4b		4	565.07	1.017	1.016	1.033	−0.031	209/8	309/54
KJ 65A.1		15	450.89	1.017	1.016	1.033	−0.026	80/11	179/40
KJ 65A.3		13	547.68	1.023	1.022	1.045	−0.019	312/48	162/38
KJ 65A.4a		6	585.4	1.018	1.022	1.04	0.113	303/50	131/40
KJ 65A.4b		5	547.86	1.017	1.024	1.041	0.173	272/32	150/41
KJ 65B		12	590.72	1.011	1.006	1.018	−0.308	108/23	234/54
KJ 66		13	600.96	1.024	1.024	1.049	−0.012	227/82	60/8
KJ 67A		15	990.09	1.007	1.004	1.011	−0.323	348/81	243/2
KJ 67B		20	1094.02	1.005	1.001	1.007	−0.627	218/8	354/79
JD 150A.1	**Jagannathpur**	3	542.9	1.006	1.001	1.007	−0.794	132/53	348/31
JD 150A.5	**Second-order Fold Hinge**	10	587.26	1.007	1.002	1.01	−0.541	118/81	225/3
JD 150B.2		13	625.55	1.01	1.006	1.016	−0.281	115/8	359/72
JD 150B.3		8	585.13	1.01	1.001	1.013	−0.759	122/7	242/76
JD 150B.4		14	621.91	1.003	1.004	1.007	0.223	114/50	255/33
JD 155.1		16	530.57	1	1.003	1.004	0.78	298/11	88/78
JD 155.2		8	427.5	1.001	1.008	1.01	0.835	342/48	124/35
JD 155.3		10	461.49	1.003	1.003	1.006	0.003	212/66	81/16
JD 155.4		20	431.68	1.001	1.001	1.002	0.268	213/81	94/4
JD 155.5		12	441.68	1.003	1.002	1.005	−0.186	286/79	80/10
JD 156.1		11	560.23	1.002	1.007	1.009	0.596	62/4	308/80
JD 156.2		8	568.79	1.002	1.004	1.006	0.449	239/3	335/63
JD 156.3		12	517.99	1.001	1.004	1.005	0.447	195/17	55/68
JD 156.4		12	562.28	1.002	1.003	1.005	0.186	260/12	5/52
JD 156.5		9	534.78	1.002	1.002	1.004	0	259/9	356/36
JD 156.6		6	516.43	1.007	1.004	1.011	−0.255	276/17	12/21
JD 157.1		8	656.71	1.005	1.004	1.009	−0.03	261/12	162/38
JD 157.2		9	739.62	1.004	1.001	1.006	−0.625	270/25	174/13
JD 157.3		8	741.35	1.003	1.002	1.006	−0.199	252/23	12/50
JD 157.4		13	865.7	1.01	1.004	1.015	−0.411	190/87	325/2
JD 157.5		8	777.04	1.007	1.003	1.011	−0.375	51/26	308/24
JD 157.6		5	799.58	1.004	1.003	1.007	−0.197	237/20	146/2
KJ 63.1	**Hinge-Eastern Anticline**	13	664.75	1.02	1.015	1.034	−0.147	260/5	358/57
KJ 63.2		11	645.77	1.021	1.017	1.039	−0.112	261/1	352/54
KJ 63.3		11	631.8	1.024	1.02	1.044	−0.084	265/4	359/48
JD 151.1	**Eastern Limb–Eastern**	13	511.05	1.003	1.003	1.006	−0.083	277/3	180/69
JD 151.2	**Anticline**	12	522.11	1.003	1.003	1.006	0.059	259/18	152/43
JD 151.3		9	563.66	1.001	1.002	1.003	0.319	122/6	231/72
JD 151.4		10	604.69	1.001	1.003	1.004	0.363	263/12	353/1
JD 151.5		13	564.48	1.002	1.005	1.007	0.385	79/8	183/58
JDE 152.1		11	570.52	1.003	1.001	1.004	−0.561	42/32	143/17
JDE 152.2		11	761.4	1.011	1.007	1.018	−0.205	253/77	148/3
JDE 152.3		12	680.97	1.009	1.003	1.012	−0.475	269/65	97/25
JDE 152.4		10	575.27	1.003	1.002	1.004	−0.224	1/22	114/44
JDE 152.5		12	632.12	1.002	1.006	1.008	0.575	1/3	92/33
JDE 155.1		6	587.28	1.005	1.006	1.01	0.106	331/49	94/25
JDE 155.2		9	547.07	1.005	1.008	1.013	0.216	227/65	110/12
JDE 155.3		7	537.76	1.005	1.007	1.012	0.212	245/47	104/36
JDE 155.4		10	598.47	1.012	1.005	1.017	−0.392	192/83	69/4
JDE 155.5		13	577.15	1.001	1.004	1.005	0.434	169/48	72/6
JDE 155.6		9	506.92	1.005	1.005	1.01	−0.068	211/73	90/9

(*continued on next page*)

Table 2 (*continued*)

Sample no.	Structural domain	N	Km ($\times 10^{-6}$ SI Unit)	L	F	P_j	T_j	K_1–D/I	K_3–D/I
JDW 153.1a	**Western Limb–Western Anticline**	4	632.15	1.015	1.025	1.041	0.257	54/74	162/5
JDW 153.1c		5	647.23	1.013	1.023	1.037	0.286	73/75	170/2
JDW 153.2		13	559.09	1.014	1.027	1.042	0.325	79/69	172/1
JDW 153.3		9	638.28	1.012	1.028	1.042	0.417	92/72	343/6
JDW 153.4		17	640.88	1.013	1.023	1.037	0.277	70/75	166/2
JDW 153.5		5	618.72	1.012	1.024	1.037	0.334	40/78	168/7
JDW 153.6		12	602.62	1.014	1.032	1.047	0.397	73/70	339/1
JDW 154.1		14	675.71	1.011	1.011	1.022	−0.023	29/42	135/16
JDW 154.2		11	653.69	1.011	1.006	1.018	−0.272	37/65	145/8
JDW 154.3		12	652.73	1.016	1.007	1.023	−0.395	32/61	288/8
JDW 154.4		14	622.12	1.012	1.012	1.024	0.005	14/64	137/15
JDW 154.5		12	637.63	1.013	1.023	1.037	0.28	57/47	154/6

The K_1, K_2 and K_3 orientation data were plotted as lower hemisphere equal area projections along with field data for that sample (Fig. 11). The AMS and field data from *limbs* and *hinges* (Fig. 11) of the folds were plotted to understand the relation between location of samples on a folded surface, orientation of field structures and AMS fabric. It was observed that irrespective of the position of the samples from limbs or hinges of the regional folds, the magnetic foliation is at a moderate to high angle to the layering (Fig. 11).

The geometry of magnetic foliations in lavas is generally in accordance with axial planar fabric of folds within the overlying BIFs. Two major planes trending NNE-SSW and E-W with variable dips can be deduced from projection diagrams of poles to magnetic foliations (Fig. 11). However, the overlying BIF unit presents a plethora of mesoscopic folds, which belong to an early NNE and later E-W set. Superimposition of these two fold sets at high angle has frequently developed typical Type-1 interference patterns in mesoscopic to macroscopic scales (Ghosh and Mukhopadhyay, 2007). Thus a gross conformity exists if the orientation of magnetic foliation planes within lava samples is viewed with respect to the axial planes of the tectonic fold sets developed within the overlying BIF.

A histogram of the average P_j values calculated from all samples was prepared (Fig. 12). It is clear from Fig. 12 that average P_j value is very low over the region. However, there is a subtle variation in the P_j values and slightly higher values have been recorded from the overturned limb and hinges in comparison to the gently dipping normal limb. Moreover average T_j values from all samples were plotted in the map (Fig. 13) to depict the distribution of the shape parameter (T_j) across the regional folds in the terrane. The distribution shows that positive and negative T_j values are more or less prevalent over specific areas indicating a domain wise change in deformation mode from flattening to constrictional types.

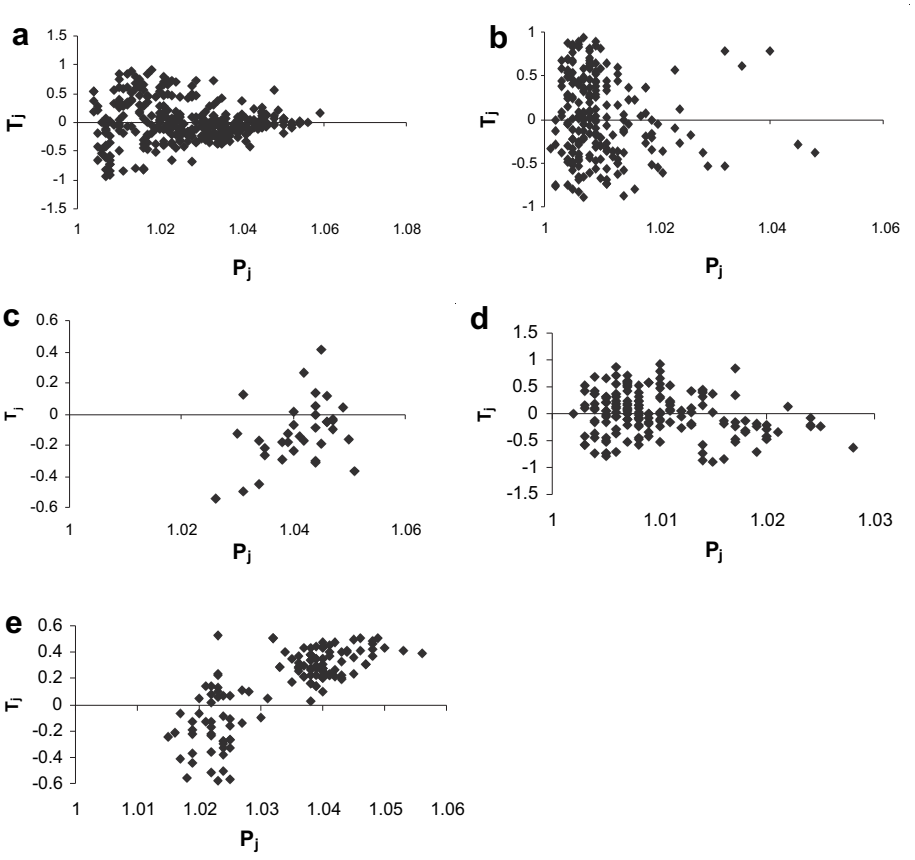

Fig. 9. Jelinek plots (Pj vs. Tj) of magnetic data of all core specimens from lava samples of the different 'Structural domains' as given in Table 1. (a) Gandhamardan second-order fold hinge. (b) Jagannathpur second-order fold hinge. (c) hinge, 'eastern anticline'. (d) eastern limb of the 'eastern anticline' and (e) western limb of the 'western syncline'.

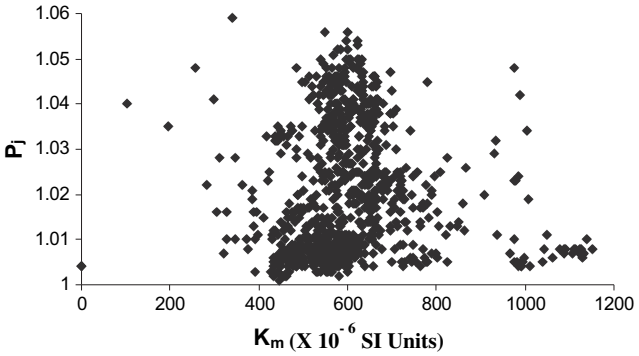

Fig. 10. Graph of degree of anisotropy (Pj) vs. mean bulk susceptibility (K_m) of 892 core specimens from 83 lava samples collected in and around the 'horseshoe synclinorium' structure, western IOG basin.

5. Discussion

5.1. AMS fabric and its origin

The low values of K_m ($<10^{-5}$ SI units) obtained from the studied samples of metabasic lavas across the regional fold structures indicate, in conformity with petrographic observations and temperature-susceptibility studies (Fig. 8), low content of ferromagnetic minerals with respect to para- and diamagnetic mineral components. Thus it could be reasonably concluded that the para- and diamagnetic fabrics played a dominant role in controlling the overall magnetic fabrics of the samples.

A low P_j value together with parallelism between primary layering and secondary magnetic foliations is believed to indicate a depositional origin of the magnetic fabric while a high P_j and moderate to very large angles between magnetic foliation and primary layering have been interpreted in terms of tectonic origin of the magnetic fabric (Tarling and Hrouda, 1993). In the present study, the P_j values are in general low for the entire area (Table 2; 1.004–1.053) and the degree of anisotropy (P_j) does not record any systematic change with increasing value of mean susceptibility (K_m; Fig. 10). The presently observed low P_j values from the lava samples are in strong contrast with the high P_j values ($\sim$1.3) obtained from the overlying strongly folded BIF unit (Mukherji et al., 2004). Mukherji et al. (2004) also reported high K_m values (720×10^{-6}–230×10^{-3} SI unit) from the BIF unit of the basin, which they ascribed primarily with the presence of magnetite within the rocks (see also Mallik et al., 1993; Das et al., 1996). Their data indicated that the high P_j values were controlled both by higher susceptibility values as well as strain. However both the degree of AMS (P_j values 1.004–1.053) and susceptibility values ($K_m < 10^{-5}$ SI units) are low in the basal lava body in contrast to the overlying co-folded BIF.

One possible way to explain the overall low P_j values from the samples is to consider that there is no significant deformation and fabric development in these lavas. However, a subtle variation in P_j values has been observed across structural domains (Fig. 12). Comparatively higher P_j values have been recorded from *hinge* and *overturned western limb* of the regional folds in contrast to lower P_j values from the *normal eastern limb* (Fig. 12). It is also observed that the orientation of pole (K_3) to the magnetic foliation (K_1–K_2) plane is at moderate to high angle to pole of primary layering (S_0) within the samples from different structural settings (Fig. 11). Thus the occurrence of magnetic foliations at high angles to the primary layering (S_0), parallel to the axial plane direction of the folds and a positive correlation in variation of P_j values with respect to structural domains have lead us to infer that the magnetic fabric, in spite of the overall low Pj values, within the lava sequence is essentially a manifestation of tectonic processes. The reorientation and recrystallization of flaky minerals defining the axial planar fabric (Fig. 7) locally developed along some fold hinges strongly supports the above inference.

It could be assumed that the low K_m values probably rendered the lavas magnetically isotopic during its eruption and primary flow. Afterwards it only supported a weak deformational overprinting of magnetic fabrics during the later successive deformation episodes, in contrast to the BIFs that registered a higher degree of anisotropy (P_j values $\sim$1.3) controlled partially by higher susceptibility values and presence of magnetite (Mukherji et al., 2004; Mallik et al., 1993; Das et al., 1996). However, the superimposition of the later deformation could also lead to reorientation of minerals in the lavas produced by the first deformation so that the net result is a reduced P_j (Tarling and Hrouda, 1993). Hence both the factors of low content of ferromagnetic minerals in the rocks or successive deformations at high angle to one another could in single or in unison have probably resulted in the observed *low* P_j values in the lava.

5.2. Implication of AMS fabric on strain and folding mechanism

Variation in P_j values exist with respect to position of the lava samples in different structural domains. The low P_j values ($\sim$1.01) are restricted to the low dipping *eastern limb* of the '*eastern anticline*' recorded by the samples JD 151, JDE 152 and JDE 155 (Fig. 12). Comparatively higher values are located at the *hinge zones* of the *secondary folds* developed on the *eastern limb* of the '*eastern anticline*' ($\sim$1.02–1.03) shown by the samples KJ 50–65 and JD 150, JD 156–158. The highest values, however, occur preferentially along the hinge zone of the eastern anticline and overturned *western limb* of the '*western syncline*' ($\sim$1.04–1.05) as displayed by the samples KJ 63 and JDW 153–154, respectively (Fig. 12).

However, as degree of anisotropy (P_j) does not record any systematic change with increasing value of mean susceptibility (K_m; Fig. 10), the variation in values of degree of anisotropy (P_j), though small, can only be explained in the light of variation of regional strain pattern in the area. The slightly higher P_j values from *hinge* and *overturned western limb* of the regional folds in contrast to lower P_j values from the *normal eastern limb* suggest that the variation in P_j values can be linked to variation in strain and ultimately to tectonic deformations, which resulted in development of fold–fault structures within the IOG rocks.

Furthermore, the observed variation in P_j values across the regional folds has a direct bearing behind the mechanism of fold development within the IOG rocks. The occurrence of higher strain values in hinges and overturned limbs compared to the normal limb of asymmetric buckle folds is a common phenomenon described from both field observations (Stewart and Alvarez, 1991; Fischer et al., 1992; Poblet and McClay, 1996; Anastasio et al., 1997; Ghosh and Saha, 2005) and theoretical and mechanical models of buckle fold development (Ramberg, 1964; Ghosh, 1966; Price, 1967; Price and Cosgroove, 1990, p. 324–329). Flexural slip with concomitant layer parallel homogeneous shortening models successfully explain such occurrence of higher strain values at hinges and overturned limbs of folds compared to the less rotated normal limbs (Ramsay and Huber, 1987, p. 457; Twiss and Moores, 1992, p. 240) than the other models like pure flexure, shear or flexural slip (Ramsay and Huber, 1987, p. 457; Twiss and Moores, 1992, p. 240). The accumulation of strain in fold hinges is a function of strain rate and tightness of hinges. If the hinges remain fixed during progressive buckle folding, strain accumulation will be more at such hinges and more rotated limbs compared to the less rotated normal limbs (Fischer et al., 1992; Fischer and Anastasio, 1994;

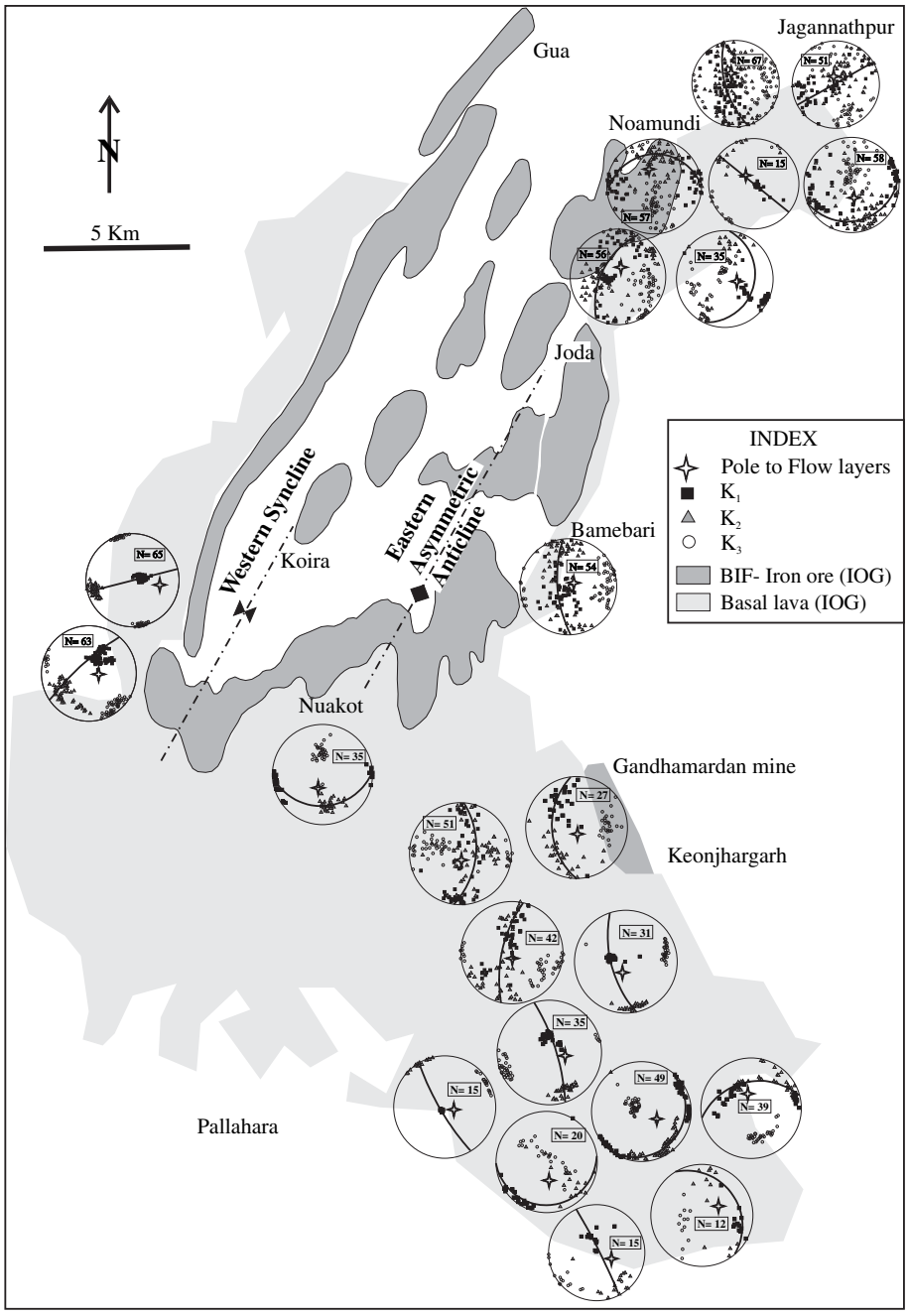

Fig. 11. Map of the 'horseshoe synclinorium' depicting the magnetic foliation trajectory in the stereographic projection diagrams of AMS directional data of all the core specimens at each site collected from lava samples as listed in Table 1 (see Fig. 1b for site locations). 'N' represents the number of core specimens at each site. The girdles in the projection diagrams represent the Magnetic foliations (F) defined by the common great circle passing through K_1 and K_2 axes of all the core specimens from samples in a single site. The pole to the 'F' is K_3. Note that the angle between K_3 and primary layering (S_0) within basal lava maintains a moderate to high angle at each sample site.

Ghosh and Saha, 2005). Thus, the variation in P_j values from lava samples correlate well with strain development in asymmetric fixed hinge buckling (concomitant flexural slip and homogeneous shortening) where higher strain values preferentially develop at the hinge and overturned limbs in contrast to the lower values at normal limbs.

5.3. Analysis of AMS fabric in the light of superposed deformation

The map view of the orientation of magnetic foliations (Fig. 11) depicts that these are consistent throughout the region defining two distinct sets (NNE and E-W) which are grossly parallel to the two sets of axial planes developed within the folded BIF. Establishment of a conformable relation between the magnetic fabric and fold superposition, however, awaits a critical evaluation of field and magnetic data. A discussion on the origin of the magnetic fabric in the lava in the light of development of the fold interference pattern within the BIF invokes proper understanding of the mutual relationships between the field and magnetic fabrics.

Detailed structural analysis from the overlying BIF have shown development of two fold sets in the IOG rocks giving rise to a typical Type-1 interference pattern in the region (Ghosh and Mukhopadhyay, 2007). The outcrop pattern of the BIF rocks is primarily

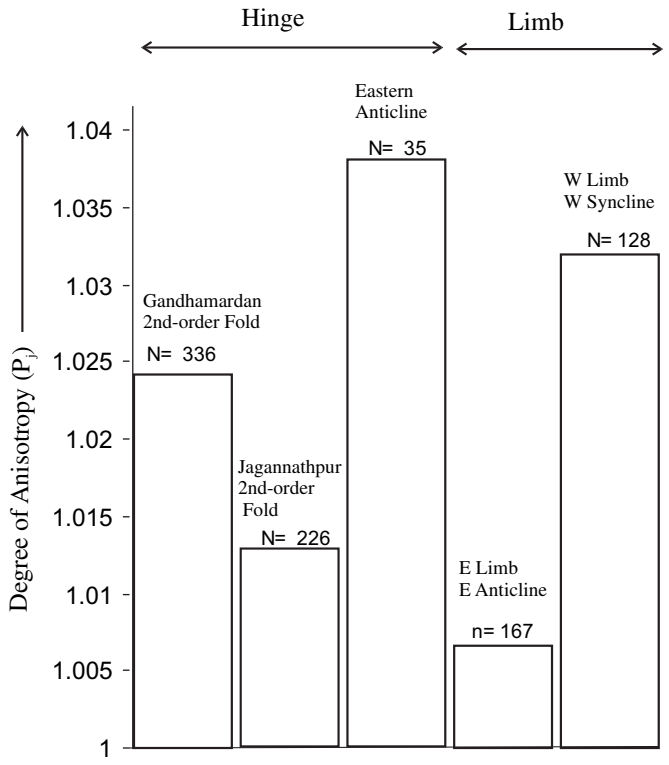

Fig. 12. Histogram comparing the degree of anisotropy (Pj) of 892 core specimens from 83 lava samples collected at 22 sites across the different 'structural domains' in the western IOG basin. 'N' represents the total number of core specimens in each 'structural domain'.

controlled by the early NNE fold set giving rise to the large-scale 'horseshoe synclinorium' structure, which in reality comprises of a fold couple of a narrow overturned *syncline* in the *west* and a broad, asymmetric *anticline* in the *east*. The later E-W folding failed to bring about any regional scale change in the spectacular horseshoe shaped outcrop of the BIF range indicating a more pervasive nature of the earlier NNE trending structural grain. However, the effect of this later E-W cross-folding is quite strong in the mesoscopic scale with frequent development of dome and basin patterns in outcrop scale. Its effect is pronounced on the '*western syncline*' in the form of development of conjugate folds on its steep western limb or by culmination and depression along the narrow axial hinge zone (Ghosh and Mukhopadhyay, 2007). However, its effect is more pronounced on the broad, sub-horizontal hinge zone of the '*eastern anticline*', where dome and basin patterns are frequent over a wide area within the BIF outcrop (Ghosh and Mukhopadhyay, 2007).

The magnetic foliation trajectories within the lava sequence in the region (Figs. 11 and 13) closely mimic the fold interference pattern developed within the BIF. The development of multiple sets of axial traces in the elongate basinal outcrop of BIF-iron ore in the Langalata iron mine (Fig. 3), at the hinge zone of the '*eastern anticline*', is very similar to the pattern of magnetic foliation trajectories prepared in course of the present analysis (Figs. 11 and 13). The map pattern of the magnetic foliation trajectories reflects that the entire outcrop of the lava sequence can be subdivided in to smaller sub-areas homogeneous with respect to the NNE (M_1 domains) and E-W set (M_2 domains) of magnetic foliations (Fig. 13). The pattern is very similar to the well trenched practice of structural analysis carried out in multiply deformed terranes where sub-areas with respect to a particular folding deformation is demarcated on the basis of dominance of a controlling fold axis or axial plane/tectonic foliation. On application of the technique of field structural analysis on the AMS data, keeping in mind the sequence of structural development within the BIF, it is possible to correlate the sub-areas with NNE magnetic foliation as M_1 (equivalent to F_1) domains and E-W magnetic foliation as M_2 (equivalent to F_2) domains. The dominance of the D_1 deformation episode over D_2 is also pronounced from the map of magnetic fabric trajectories (Fig. 13) reflected by the large spatial extent of the F_1 magnetic fabric (M_1 domains) in contrast to narrow deformation zones (M_2 domains) where the E-W magnetic fabric is prevailing. The frequent swing in the NNE magnetic grain to NE, N or NNW trends (Fig. 13) against the back-drop of consistent orientation of the E-W fabric strongly supports modification of the earlier episode of NNE-SSW deformational grain by the later episode of E-W deformation. The contention is in compliance with the established deformation sequence in the region formulated on the basis of rigorous structural analysis from BIF–phyllite–shale (Ghosh and Mukhopadhyay, 2007). It further indicates that even the sequence of development of the successive magnetic fabrics, if any, could also be established from careful systematic mapping of the magnetic fabrics in regional scale as done in the present analysis.

The Jelinek plots of P_j vs. T_j values (Fig. 9) indicate an oblate to prolate shape of the susceptibility ellipsoid. Thus the overall nature of deformation varies from constrictional to flattening type in the region. The variation in magnitude of T_j values within the lava outcrop depicts an interesting pattern as well (Fig. 13). In spite of apparent aberrations at places, the positive T_j values preferentially concentrate in M_1 magnetic domains. The higher T_j values gradually diminishes as the narrow M_2 magnetic domains are approached with ultimate dominance of negative T_j values in M_2 domains. The observations have a direct bearing on the nature of strain accumulation during the multiple deformation episodes within the IOG rocks. The preferential occurrence of positive T_j values in the NNE-SSW trending M_1 domains indicates that the nature of earlier D_1 deformation was of flattening type with gross E-W shortening being accommodated through concomitant extensions in a sub-vertical as well N-S sub-horizontal direction, parallel to the axes of the F_1 folds. The later E-W cross-folding (D_2 deformation) was achieved mainly through the N-S shortening episode during which typical Type-1 interference patterns were produced. The D_1 strain pattern within the rocks is bound to get modified depending upon the intensity of D_2 deformation as well as on the nature of overall strain development, i.e., whether the resultant strain is homogeneous or heterogeneous in regional scale. The preferential occurrence of negative T_j values in M_2 domains thus further indicate that the initial flattening strain of the D_1 deformation were progressively modified to an overall constrictional strain in narrow D_2 domains by the later N-S shortening episode (D_2 deformation).

6. Conclusions

Structural analysis in deformed low-grade metalava is a challenge in absence of common deformation fabrics such as mesoscopic fold, foliation, lineation or any strain markers. Despite the above inherent difficulties, the present study highlights that the AMS data can be used as an effective tool for assessing strain variation and identification of deformation fabrics from a low-grade greenstone metalava succession. The metalava in the present study area grossly lack development of mesoscopic folds or penetrative axial planar fabrics, excepting locally. However, the lava yields magnetic foliations that lie at moderate to high angle with the flow layers implying their tectonic origin. Although the degree of magnetic anisotropy (P_j) is low throughout the region, the above line of reasoning negates the possibility that the lavas are grossly undeformed. Two distinct sets of magnetic foliations recorded from

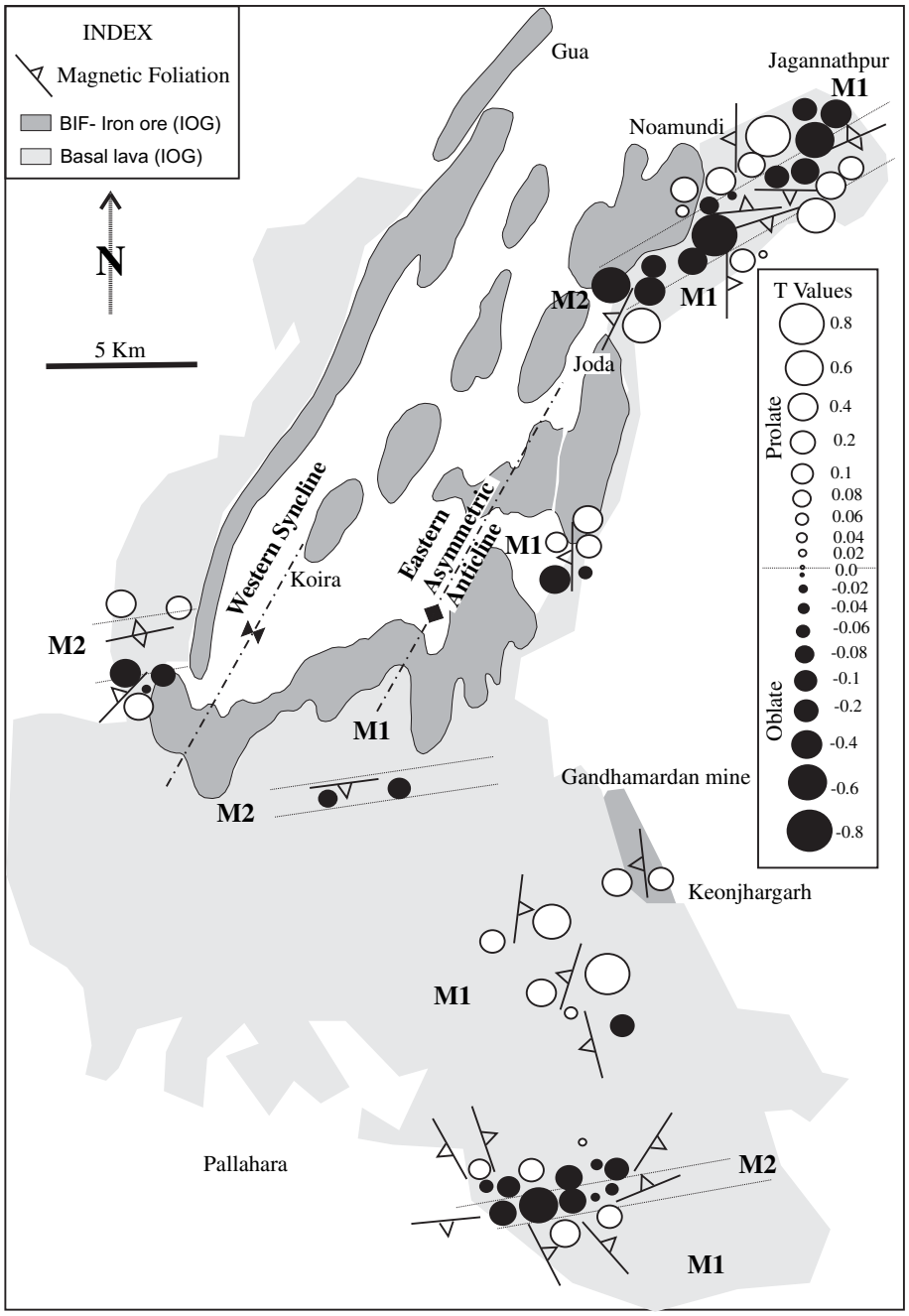

Fig. 13. Map of the 'horseshoe synclinorium' showing the mean magnetic foliation trajectory and distribution of mean values of shape parameter (Tj) from each sample as listed in Table 2 (similar mean Tj values for samples from a particular site are represented by a single value in the map). Note the preferential concentration of '−ve T' values in narrow M_2 domains indicating prevalence of constrictional strain state in M_2 domains.

the lava correlate well with the axial plane directions of the two sets of folds developed within the overlying co-folded BIF unit. Variation in P_j and T_j values has been correlated with specific structural domains within the regional folds. Thus in spite of absence of suitable strain markers, the magnetic parameters (P_j and T_j) determined from AMS studies record the strain variation across the belt, which otherwise would have been gone unnoticed. It is not a usual practice to apply AMS techniques in analyzing superposed deformation fabrics from a region. The significance of the present study lies in this perspective, which highlights the potential of the AMS technique in unraveling multiple deformation events from strata that do not apparently exhibit megascopic evidences for superposed deformations.

Acknowledgements

This work is a part of the Department of Science and Technology, India, sponsored Major Research Project (no. ESS/16/229/2005). The AMS analysis has been carried out at the Indian Institute of Geomagnetism (IIGM), Alibagh and Allahabad, India and the authors are thankful to the Director, IIGM for his kind cooperation. We acknowledge hospitality extended by the Tata Steel, Joda, and the Rungta Mines, Jajang during the field programme. Helpful suggestions and comments by F. Hrouda, Ian Alsop and two anonymous reviewers have substantially improved the manuscript. We highly appreciate the thought provoking editorial comments and suggestions from Joao Hippertt. We also acknowledge the DST-

FIST and UGC-CAS laboratory facility of the Geology Department, Presidency College, Kolkata.

References

Anastasio, D.J., Fischer, D.M., Messina, T.A., Holl, J.E., 1997. Kinematics of de'collement folding in the Lost River Range, Idaho. Journal of Structural Geology 19, 355–368.

Archanjo, C.J., Bouchez, J.L., Corsini, M., Vauchez, A., 1994. The Pombal granite pluton: magnetic fabric, emplacement and relationships with the Brasiliano strike–slip setting of NE Brazil (Paraiba State). Journal of Structural Geology 16, 323–335.

Acharyya, S.K., 1993. Greenstones from Singhbhum craton, their Archean character, oceanic crust affinity and tectonics: In: Proceedings of National Academy of Science, India, Sec A 63, 211–222.

Basu, A.R., Bandyopadhyay, P.K., Chakrabarti, R., Zou, H., 2008. Large 3.4 Ga Algoma-type BIF in the Eastern Indian Craton. Geochimica et Cosmochimica Acta, 72(12S- Goldschmidt 2008 Conference Abstract Volume), A59.

Beukes, N.J., Mukhopadhyay, J., Gutzmer, J., 2008. Genesis of high-grade Iron Ores of the Archean Iron Ore Group around Noamundi, India. Society of Economic Geologists 103, 365–386.

Borradaile, G.J., Henry, B., 1997. Tectonic applications of magnetic susceptibility and its anisotropy. Earth Science Review 42, 49–93.

Borradaile, G.J., Jackson, M., 2004. Anisotropy of magnetic susceptibility (AMS): magnetic petrofabrics of deformed rocks. In: Martin-Hernandez, F., Luneburg, C.M., Aubourg, C., Jackson, M. (Eds.), Magnetic fabric: methods and applications. Geological Society, London, Special Publications, vol. 238, pp. 299–360.

Borradaile, G.J., Lagroix, F., King, D., 1998. Tilting and transpression of an Archean anorthosite in northern Ontario. Tectonophysics 293, 239–254.

Bouchez, J.L., Gleizes, G., Djouadi, T., Rochette, P., 1990. Microstructure and magnetic susceptibility applied to emplacement kinematics of granites: the example of the Foix pluton (French Pyrenees). Tectonophysics 184, 157–171.

Bouchez, J.L., 1997. Granite is never isotropic: an introduction to AMS studies of granitic rocks. In: Bouchez, J.L., Hutton, D.W.H., Stephens, W.E. (Eds.), Granite: from segregation of melt to emplacement fabrics. Kluwer, Dordrecht, Netherlands, pp. 95–112.

Chatterjee, A.K., Mukherjee, P., 1981. The structural set up of a part of the Malangtoli iron ore deposits, Orissa. Journal Geological Society of India 22, 121–130.

Das, A.K., Piper, J.D.A., Mallik, S.B., Sherwood, G.J., 1996. Palaeomagnetic study of Archaean Banded Hematite Jasper Rocks from the Singhbhum–Orissa Craton, India. Precambrian Research 80, 193–204.

de Wall, H., Greiling, R.O., Sadek, M.F., 2001. Post-collisional shortening in the late Pan-African Hamisana high strain zone, SE Egypt: field and magnetic fabric evidence. Precambrian Research 107, 79–194.

Djouadi, M.T., Gleizes, G., Ferré, E., Bouchez, J.L., Caby, R., Lesquer, A., 1997. Oblique magmatic structures of two epizonal granite plutons, Hoggar, Algeria: late-orogenic emplacement in a transcurrent orogen. Tectonophysics 279, 351–374.

Dunn, J.A., 1929. The geology of north Singhbhum including parts of Ranchi and Manbhum districts. Memoir Geological Survey of India 54 (2).

Dunn, J.A., 1940. The stratigraphy of south Singhbhum. Memoir Geological Survey of India 63, 281–450.

Ferré, E., Gleizes, G., Caby, R., 2002. Obliquely convergent tectonics and granite emplacement in the Trans-Saharan belt of Eastern Nigeria—a synthesis. Precambrian Research 114, 199–219.

Fischer, M.P., Woodward, N.B., Mitchell, M.M., 1992. The kinematics of break-thrust folds. Journal of Structural Geology 14, 451–460.

Fischer, M.P., Anastasio, D.J., 1994. Kinematic analysis of a large scale leading edge fold, Lost River Range, Idaho. Journal of Structural Geology 16, 337–364.

Ghosh, G., Mukhopadhyay, J., 2007. Reappraisal of the structure of the Western Iron Ore Group, Singhbhum craton, eastern India: Implications for the exploration of BIF-hosted iron ore deposits. Gondwana Research 12, 525–532.

Ghosh, G., Saha, D., 2005. Kinematics of large scale asymmetric folds and associated smaller scale brittle–ductile structures in the Proterozoic Somnur Formation, Pranhita–Godavari valley, south India. Journal of Earth System Science 114, 125–142.

Gleizes, G., Leblanc, D., Oliver, P., Bouchez, J.-L., 2001. Strain partitioning in a pluton during emplacement in a transpressional regime: the example of the Neoville Granite (Pyrenees). International Journal of Earth Sciences 90, 325–340.

Ghosh, S.K., 1966. Experimental tests of buckling folds in relation to strain ellipsoid in simple shear deformations. Tectonophysics 3, 169–185.

Ghosh, S.K., Mandal, N., Khan, D., Deb, S.K., 1992. Modes of superposed buckling in single layers controlled by initial tightness of early folds. Journal of Structural Geology 14, 381–394.

Ghosh, S.K., Mandal, N., Sengupta, S., Khan, D., Deb, S.K., 1993. Superposed buckling in multilayers. Journal of Structural Geology 15, 95–111.

Hrouda, F., 1978. The magnetic fabric in some folds. Physics of Earth and Planetary Interiors 17, 89–97.

Hrouda, F., 1993. Theoretical models of magnetic anisotropy to strain relationship revisited. Physics of the Earth and Planetary Interiors 77, 237–249.

Hrouda, F., Krejči, O., Otava, J., 2000. Magnetic fabrics in folds of the Eastern Rheno-Hercynian Zone. Physics and Chemistry of the Earth (A) 25, 505–510.

Jayangondaperumal, R., Dubey, A.K., 2001. Superposed folding of a blind thrust and formation of klippen: results of anisotropic magnetic susceptibility studies from the Lesser Himalaya. Journal of Asian Earth Sciences 19, 713–725.

Jones, H.C., 1934. The iron ore deposits of Bihar and Orissa. Memoir Geological Survey of India 63 (2), 167–302.

Jelinek, V., 1981. Characterization of the magnetic fabric of rocks. Tectonophysics 79, T63–T67.

Leblanc, D., Gleizes, G., Roux, L., Bouchez, J.L., 1996. Variscan dextral transpression in the French Pyrenees: new data from the Pic des Trois-Seigneurs granodiorite and its country rocks. Tectonophysics 261, 331–345.

Mallik, S.B., Sherwood, G.J., Das, A.K., 1993. The magnetic mineralogy of the Precambrian Banded Hematite Jasper Formation, Orissa, India. Journal of Geomagnetism and Geoelectricity 45, 155–165.

Mamtani, M.A., Greiling, R.O., Karanth, R.V., Merh, S.S., 1999. Orogenic deformation and its relationship to AMS fabric—an example from the southern margin of the Aravalli Mountain Belt, India. In: Radhakrishna, T., Piper, J.D. (Eds.), The Indian Subcontinent and Gondwana: a Palaeomagnetic and Rock Magnetic Perspective. Geological Society of India Memoir, 44, pp. 9–24.

Misra, S., 2006. Precambrian chronostratigraphic growth of Sighbhum–Orissa craton, eastern Indian shield; an alternative model. Journal Geological Society of India 67, 356–378.

Mukherji, A., Chaudhuri, A.K., Mamtani, M.A., 2004. Regional scale strain variations in Banded Iron Formations of eastern India: results from anisotropy of magnetic susceptibility studies. Journal of Structural Geology 26, 2175–2189.

Mukhopadhyay, D., 2001. The archaean nucleus of Singhbhum: the present state of knowledge. Gondwana Research 4, 307–318.

Mukhopadhyay, J., Beukes, N.J., Armstrong, R.A., Zimmermann, U., Ghosh, G., Medda, R.A., 2008. Dating the Oldest Greenstone in India: A 3.51 Ga Precise U-Pb SHRIMP Zircon Age for Dacitic Lava of the Southern Iron Ore Group, Singhbhum Craton. Journal of Geology 116, 449–461.

Naqvi, S.M., 2005. Geology and evolution of the Indian Plate (from Hadean to Holocene: 4 Ga to 4 Ka). Capital Publishing, New Delhi.

Neves, S.P., Araujo, A.M.B., Correia, P.B., Mariano, G., 2003. Magnetic fabrics in the Cabanas Granite (NE Brazil) Interplay between emplacement and regional fabrics in a dextral transpressive regime. Journal of Structural Geology 25, 441–453.

Parada, M.A., Roperch, P., Guiresse, C., Ramírez, E., 2005. Magnetic fabrics and compositional evidence for the construction of the Caleu pluton by multiple injections, Coastal Range of central Chile. Tectonophysics 399, 399–420.

Paul, D.K., Mukhopadhyay, D., Pyne, T.K., Bishui, P.K., 1991. Rb–Sr age of granitoid in the Deo River section, Singhbhum and its relevance to the age of iron formation. Indian Minerals 45, 726–728.

Poblet, J., McClay, K., 1996. Geometry and kinematics of single layer detachment folds. American Association of Petroleum Geologists Bulletin 80, 1085–1109.

Price, N.J., 1967. The initiation and development of asymmetric buckle folds in non-metamorphosed competent sediments. Tectonophysics 4, 173–201.

Price, N.J., Cosgroove, J.W., 1990. Analysis of geological structures. Cambridge University Press, New York.

Ramberg, H., 1964. Selective buckling of composite layers with contrasted rheological properties, a theory for the formation of several orders of folds. Tectonophysics 1, 307–341.

Ramsay, J.G., 1967. Folding and Fracturing of Rocks. McGraw-Hill Book Company, New York.

Ramsay, J.G., Huber, M.I., 1987. The techniques of modern structural geology. In: Folds and Fractures, vol. 2. Academic Press, London.

Saha, A.K., 1994. Crustal evolution of Singhbhum-North Orissa, eastern India. Geological Society of India Memoir 27, 1–341.

Sarkar, S.C., 2000. Crustal evolution and metallogeny in the eastern Indian craton. Geological Survey of India Special Publication 55, 169–194.

Sarkar, S.N., Saha, A.K., 1962. A revision of the Precambrian stratigraphy and tectonics of Singhbhum and adjacent regions. Quarterly Journal of the Geological Mining and Metallurgical Society of India 34, 97–136.

Sen, K., Majumder, S., Mamtani, M.A., 2005. Degree of magnetic anisotropy as a strain intensity gauge in ferromagnetic granites. Journal of the Geological Society, London 162, 583–586.

Sen, K., Mamtani, M.A., 2006. Magnetic fabric, shape preferred orientation and regional strain in granitic rocks. Journal of Structural Geology 28, 1870–1882.

Sengupta, S., Acharyya, S.K., de Smeth, J.B., 1997. Geochemistry of Archean volcanic rocks from Iron Ore Supergroup, Singhbhum, eastern India. Proceedings Indian Academy of Science 106, 327–342.

Sengupta, S., Ghosh, S.K., Deb, S.K., Khan, D., 2005. Opening and closing of folds in superposed deformations. Journal of Structural Geology 27, 1282–1299.

Simon, J.L., 2004. Superposed buckle folding in the eastern Iberian chain, Spain. Journal of Structural Geology 26, 1447–1664.

Stewart, K.G., Alvarez, W., 1991. Mobile-hinge kinking in layered rocks and models. Journal of Structural Geology 13, 243–259.

Tarling, D.H., Hrouda, F., 1993. The magnetic anisotropy of rocks. Chapman and Hall, London.

Thiessen, R.L., Means, W.D., 1980. Classification of fold interference patterns: a reexamination. Journal of Structural Geology 2, 311–316.

Turner, F.J., Weiss, L.E., 1963. Structural analysis of metamorphic tectonites. McGraw Hill, New York.

Twiss, R.J., Moores, E.M., 1992. Structural Geology. W.H. Freeman, New York.